UCSF
UC San Francisco Previously Published Works

Title
Multimodal molecular analysis of astroblastoma enables reclassification of most cases into more specific molecular entities.

Permalink
https://escholarship.org/uc/item/30q3s25n

Journal
Brain pathology (Zurich, Switzerland), 28(2)

ISSN
1015-6305

Authors
Wood, Matthew D
Tihan, Tarik
Perry, Arie
et al.

Publication Date
2018-03-01

DOI
10.1111/bpa.12561

Peer reviewed

eScholarship.org Powered by the California Digital Library
University of California

Brain Pathology ISSN 1015–6305

RESEARCH ARTICLE

Multimodal molecular analysis of astroblastoma enables reclassification of most cases into more specific molecular entities

Matthew D. Wood [1]; Tarik Tihan[1]; Arie Perry[1,2]; Geeta Chacko[3]; Clinton Turner[4]; Cunfeng Pu[5]; Christopher Payne[6]; Alexander Yu[6]; Serguei I. Bannykh[7]; David A. Solomon [1]

[1] Department of Pathology, Division of Neuropathology, [2] Department of Neurological Surgery, University of California, San Francisco, CA.
[3] Department of Pathology, Division of Neuropathology, Christian Medical College, Vellore, Tamil Nadu, India.
[4] Anatomical Pathology, LabPLUS Auckland City Hospital, Auckland, New Zealand.
[5] Department of Pathology, [6] Department of Neurosurgery, Allegheny General Hospital, Pittsburgh, PA.
[7] Department of Pathology and Laboratory Medicine, Cedars-Sinai Medical Center, Los Angeles, CA.

Keywords
astroblastoma, CNS-HGNET-*MN1*, DNA methylation profiling, next-generation sequencing.

Corresponding author:
David A. Solomon, MD, PhD, Division of Neuropathology, Department of Pathology, University of California San Francisco, 513 Parnassus Ave, Health Sciences West 451, San Francisco, CA 94143 (E-mail: *David.Solomon@UCSF.edu*)

Received 25 August 2017
Accepted 14 September 2017
Published Online Article Accepted 28 September 2017

doi:10.1111/bpa.12561

Abstract

Astroblastoma is a rare and controversial glioma with variable clinical behavior. The diagnosis currently rests on histologic findings of a circumscribed glioma with astroblastomatous pseudorosettes and vascular hyalinization. Immunohistochemical studies have suggested different oncogenic drivers, such as *BRAF* p.V600E, but very few cases have been studied using genome-wide methodologies. Recent genomic profiling identified a subset of CNS embryonal tumors with astroblastoma-like morphology that harbored *MN1* gene fusions, termed "CNS high-grade neuroepithelial tumors with *MN1* alteration" (CNS-HGNET-*MN1*). To further characterize the genetic alterations that drive astroblastomas, we performed targeted next-generation sequencing (NGS) of 500 cancer-associated genes in a series of eight cases. We correlated these findings with break-apart fluorescence in situ hybridization (FISH) analysis of the *MN1* locus and genome-wide DNA methylation profiling. Four cases showed *MN1* alteration by FISH, including two pediatric cases that lacked other pathogenic alterations, and two adult cases that harbored other cancer-associated gene mutations or copy number alterations (eg, *CDKN2A/B* homozygous deletion, *TP53*, *ATM* and *TERT* promoter mutations). Three of these cases grouped with the CNS-HGNET-*MN1* entity by methylation profiling. Two of four *MN1* intact cases by FISH showed genetic features of either anaplastic pleomorphic xanthoastrocytoma (*BRAF* p.V600E mutation, *CDKN2A/B* homozygous deletion and *TERT* promoter mutation) or IDH-wildtype glioblastoma (trisomy 7, monosomy 10, *CDK4* amplification and *TP53*, *NRAS* and *TERT* promoter mutations) and these cases had an aggressive clinical course. Two clinically indolent cases remained unclassifiable despite multimodal molecular analysis. We conclude that astroblastoma histology is not specific for any entity including CNS-HGNET-*MN1*, and that additional genetic characterization should be considered for astroblastomas, as a number of these tumors likely contain a methylation profile or genetic alterations that suggest classification as other tumor entities. Our heterogeneous molecular findings help to explain the clinical unpredictability of astroblastoma.

INTRODUCTION

Astroblastoma is a rare, circumscribed glial neoplasm, first described by Bailey and Cushing in the early 20th century and further characterized by Bailey and Bucy in 1930 (3, 4). According to the World Health Organization (WHO), the diagnosis rests on identifying a key histologic feature: extensive perivascular pseudorosettes with thickened, stout or non-tapering cell processes, which are often but not invariably accompanied by focal or extensive sclerosis/hyalinization, usually involving blood vessels (20). Most tumors are immunoreactive for glial fibrillary acidic protein (GFAP) and lack a diffusely infiltrating component. Due to the rarity of this tumor and its unpredictable outcome, the 2016 WHO Classification does not currently assign a grade to this entity (20). Although most neuropathologists separate these tumors into well differentiated or anaplastic/malignant forms, there is not a universal criterion for making this distinction (8, 9). Problematically, even within the low- and high-grade categories, the clinical behavior is highly variable (1, 13, 17, 27).

© 2017 International Society of Neuropathology

Very few cases of astroblastoma have been studied using modern molecular techniques. One next-generation sequencing study of three cases identified mutations in a few genes known to be altered in low-grade gliomas, including *BCOR*, *BCORL1*, *ERBB3*, *MYB* and *ATM*, but no recurrent mutations were seen (5). Importantly, this study did not identify mutations in genes that are commonly altered in infiltrating astrocytoma, such as *IDH1*, *ATRX* or *TP53*, thus differentiating astroblastoma genetically from diffuse gliomas and validating previous immunohistochemical findings (2). In another immunohistochemical study of 28 cases, Lehman *et al* identified *BRAF* p.V600E mutant protein in 38% of cases, raising the possibility of genetic overlap between astroblastoma and other circumscribed glial neoplasms driven by MAPK pathway alterations such as pleomorphic xanthoastrocytoma, ganglioglioma and pilocytic astrocytoma (19). Other genetic studies of astroblastoma, including array comparative genomic hybridization, have not identified a recurrent, signature genetic abnormality, but have served to distinguish astroblastoma from conventional diffuse glioma or ependymoma (9).

Recently, an application of DNA methylation profiling to a series of supratentorial central nervous system embryonal neoplasms identified a distinct methylation cluster defined by recurrent rearrangements involving the meningioma 1 (*MN1*) gene on chromosome 22q (25). Surprisingly, 39% of these "CNS high-grade neuroepithelial tumors with *MN1* alteration" (CNS-HGNET-*MN1*) cases showed histologic features of astroblastoma, and a majority of tumors with astroblastoma histology in the study fell into the CNS-HGNET-*MN1* cluster of tumors. This raised the possibility that some tumors diagnosed as astroblastoma using WHO criteria harbor *MN1* alterations. Nevertheless, astroblastoma histology was clearly not a defining characteristic for CNS-HGNET-*MN1*, as the majority of cases in this DNA methylation cluster lacked characteristic astroblastoma histology (25). This finding, taken along with the prior genetic studies of astroblastoma, raises the possibility that "astroblastoma" is a morphologic pattern that can be seen across a spectrum of molecular entities.

To advance our understanding of the molecular features that define these challenging cases, we applied a targeted next-generation sequencing panel covering approximately 500 tumor-associated genes to a series of circumscribed gliomas with a pathologic diagnosis of astroblastoma. Here, we describe the histologic, immunophenotypic and genetic features in this series, and correlate our findings with breakapart fluorescence in situ hybridization (FISH) assessment of the *MN1* locus and tumor classification by whole genome DNA methylation profiling.

METHODS

Cases were identified by electronic search of the University of California San Francisco (UCSF) pathology records, including both in-house and consultation cases. Clinical histories were extracted by review of the patient electronic medical records, and by discussion with the referring pathologist when applicable. Tumor histologic features were extracted from the clinical reports and confirmed by microscopic analysis of the available hematoxylin and eosin (H&E)-stained slides. This work was conducted under supervision of the University of California San Francisco Institutional Review Board.

Tumor histologic features and immunophenotype were compiled from examination of available clinical slides, and by performing additional immunohistochemical stains in select cases. Immunohistochemical stains performed at UCSF included GFAP (DAKO rabbit polyclonal, 1:3000), oligodendrocyte transcription factor 2 (OLIG2, Immuno Bio Labs rabbit polyclonal, 1:200), epithelial membrane antigen (EMA, Leica clone Gp1.4, prediluted), neurofilament (NFIL, Cell Marque clone 2F11, undiluted) and L1 cell adhesion molecule (L1CAM, Sigma clone UJ127.11, 1:1800).

For the genetic analysis, genomic DNA was isolated from tumor tissue collected by microdissection from unstained slides, or by punching blocks of formalin-fixed paraffin-embedded tissue. DNA was extracted using a Qiagen DNEasy FFPE DNA extraction kit (Hilden, Germany). The UCSF 500 Cancer Gene Panel and its application to neuro-oncology patients has been described previously (14). Briefly, after genomic DNA library preparation, barcoding and hybrid capture-based target enrichment, next-generation sequencing was performed on an Illumina HiSeq 2500 instrument (San Diego, CA, USA). This yielded sequence data from the coding regions of 510 cancer-associated genes, the *TERT* promoter and selected introns from 40 genes to detect common gene rearrangements (14). Sequencing of intergenic regions at regular intervals across the genome enabled chromosomal copy number assessment. The total sequencing footprint is approximately 2.8 MB.

The sequencing data was reviewed by two of the investigators (MDW and DAS) and alterations were classified for potential pathogenicity based on sequence coverage, tumor mutant allele frequency, reported occurrence in other neoplasms (based on COSMIC and cBioPortal databases) and frequency in human populations (based on the 1000 Genomes Project and Exome Sequencing Project 6500 databases). Focal copy number alterations and whole chromosomal gains/losses were computed from UCSF 500 sequencing data (26).

DNA methylation profiling was performed at the German Cancer Research Center in the Department of Pathology at Heidelberg University Hospital in Germany, using methods and analysis described by Korshunov *et al* and Sturm *et al* (15, 25).

FISH to assess the *MN1* locus was performed using automated techniques for deparaffinization on a VP 2000 processor and slide pretreatment on a ThermoBrite system (Abbott Molecular, Des Plaines, IL, USA). Dual color CytoOrange and CytoGreen labeled FISH probes flanking the *MN1* locus (catalog number CT-PAC112) were purchased from CytoTest, Inc. (Rockville, MD, USA) and applied in accordance to the manufacturer's instructions. Nuclei were counterstained with 4′,6-diamidino-2-phenylindole (DAPI). Slides were analyzed using a BX-41 microscope (Olympus Corporation, Center Valley, PA, USA) coupled to a CV-M4 + CL progressive scan camera for image capture (JAI, San Jose, CA, USA). A minimum of 100 tumor nuclei were evaluated for separation of the *MN1* probe signals. Two cases of medulloblastoma and one case of a central nervous system neuroblastoma with *FOXR2* rearrangement were included as negative controls (*MN1* intact). Nuclei with overlapping (ie, yellow) or closely approximated red/green signals (defined as within 1 probe width of each other) were considered to have an intact *MN1* locus. Nuclei with separated red and green signals (ie, greater than one probe width apart) or an isolated red or isolated green signal were considered to have disruption of the *MN1* locus. Tumor nuclei were only scored if at least one red and one green signal were present.

© 2017 International Society of Neuropathology

Table 1. Clinical features of astroblastoma cases. Abbreviations: AWSD = alive with stable disease; DOD = died of disease; LTFU = lost to follow-up.

Case	Age at diagnosis (years)	Gender	Tumor location	Diagnosis	Material studied	Procedure	Treatment	Clinical course	Clinical outcome, follow-up
1	35	Male	Left frontal	Recurrent astroblastoma, high grade	First recurrence (age 45)	Biopsy	Radiation, after first recurrence	Multiple local recurrences	DOD, 15.4 years
2	68	Female	Left parietal	Astroblastoma with atypia	Primary	Resection	Radiation	No recurrence	LTFU, 8.3 years (died of unknown cause at 9.8 years)
3	9	Female	Right frontal	Recurrent astroblastoma	Third recurrence (age 31)	Resection	Radiation, after first recurrence	Multiple local recurrences	AWSD, 27 years
4	10	Female	Left parietal	Anaplastic astroblastoma	Primary	Resection	Radiation and Temozolomide	No recurrence	AWSD, 2.8 years
5	25	Male	Left temporal	Anaplastic astroblastoma	Primary	Resection	Radiation	Rapid recurrence	DOD, 2 years
6	33	Male	Right frontal	Malignant astroblastoma	Primary	Biopsy	Radiation and Temozolomide	No recurrence	AWSD, 8.2 years
7	73	Male	Left occipital	Anaplastic astroblastoma	Primary	Biopsy	Radiation	Rapid recurrence	DOD, 2 years
8	31	Female	Left parietal	Malignant glioma, features suggestive of astroblastoma	Primary	Resection	Radiation and Temozolomide	No recurrence	AWSD, 1 year

RESULTS

Clinical and histologic features

Electronic search of the University of California San Francisco pathology records revealed a diagnosis of astroblastoma or anaplastic/malignant astroblastoma on 23 tumor specimens (6 in-house cases and 17 consultation specimens). Seven of these cases had tumor tissue available for study. Material from one additional case was obtained from unstained slides that were originally sent to UCSF for a research study (Case 6). Astroblastoma histologic features were confirmed by the investigators (MDW, TT, AP and DAS). Cases 6 and 7 in this series have been previously published as case reports (6, 23).

The clinical features of the cohort are summarized in Table 1. All tumors were supratentorial and cortically based, and occurred across an age range from 9 to 73 years in four male and four female patients. Molecular analysis was performed on a biopsy or resection specimen of the primary tumor for six of the cases, and on recurrent tumor in two of the cases. Treatments varied from postoperative radiation and temozolomide after the initial resection, to radiation treatment only, applied either after the initial resection or at the first tumor recurrence. The clinical outcome was highly variable. For example, in Cases 1 and 3 the patients had multiple local recurrences and repeat resections over one or more decades, while in Cases 5 and 7, the patients had rapid local tumor recurrence resulting in death in less than 2 years. None of the patients had cerebrospinal fluid dissemination.

Representative H&E-stained images are shown in Figure 1. All of the tumors showed a predominantly solid growth pattern, as evidenced on H&E stains by a lack of entrapped cortical neurons and a sharply demarcated border with adjacent brain tissue. The solid growth pattern in all tumors was supported by absence of neurofilament-positive entrapped axons on immunohistochemistry (data not shown). All tumors showed perivascular pseudorosettes with a spectrum of stout/thickened cell processes radiating toward the central vessels. In Case 5, the perivascular cell processes were relatively delicate and short, and the tumor was characterized by clustering of primitive-appearing tumor cells around blood vessels. All but two tumors showed either prominent hyalinized blood vessels or regions of tumor with ribbons of hyalinization associated with nests and cords of tumor cells. In Case 5 (a resection) and Case 7 (a biopsy), convincing hyalinization was not seen; in these cases the diagnosis of astroblastoma was based on findings of a solid glial neoplasm with astroblastomatous perivascular rosettes, and exclusion of other diagnostic possibilities based on the histology and immunoprofile.

The immunohistochemical features of the tumors are summarized in Table 2 and pictured in *Supporting Information* Figure S1. Cases 3 and 8 showed a combination of widespread immunoreactivity for OLIG2 coupled with relatively few GFAP-positive tumor cells (Figure 2A, top), while five cases showed strong reactivity for GFAP combined with significant OLIG2 staining (Cases 1, 2 and 7) or less commonly, negative OLIG2 (cases 4 and 6, Figure 2A, bottom). Case 5 was negative for OLIG2 and had only rare widely scattered GFAP-positive tumor cells. The EMA stain was highly variable across cases (Figure 2B), ranging from patchy cytoplasmic and paranuclear dot-like staining (as seen in Case 8), to a mixture of cytoplasmic, membranous and paranuclear dot-like staining (as

© 2017 International Society of Neuropathology

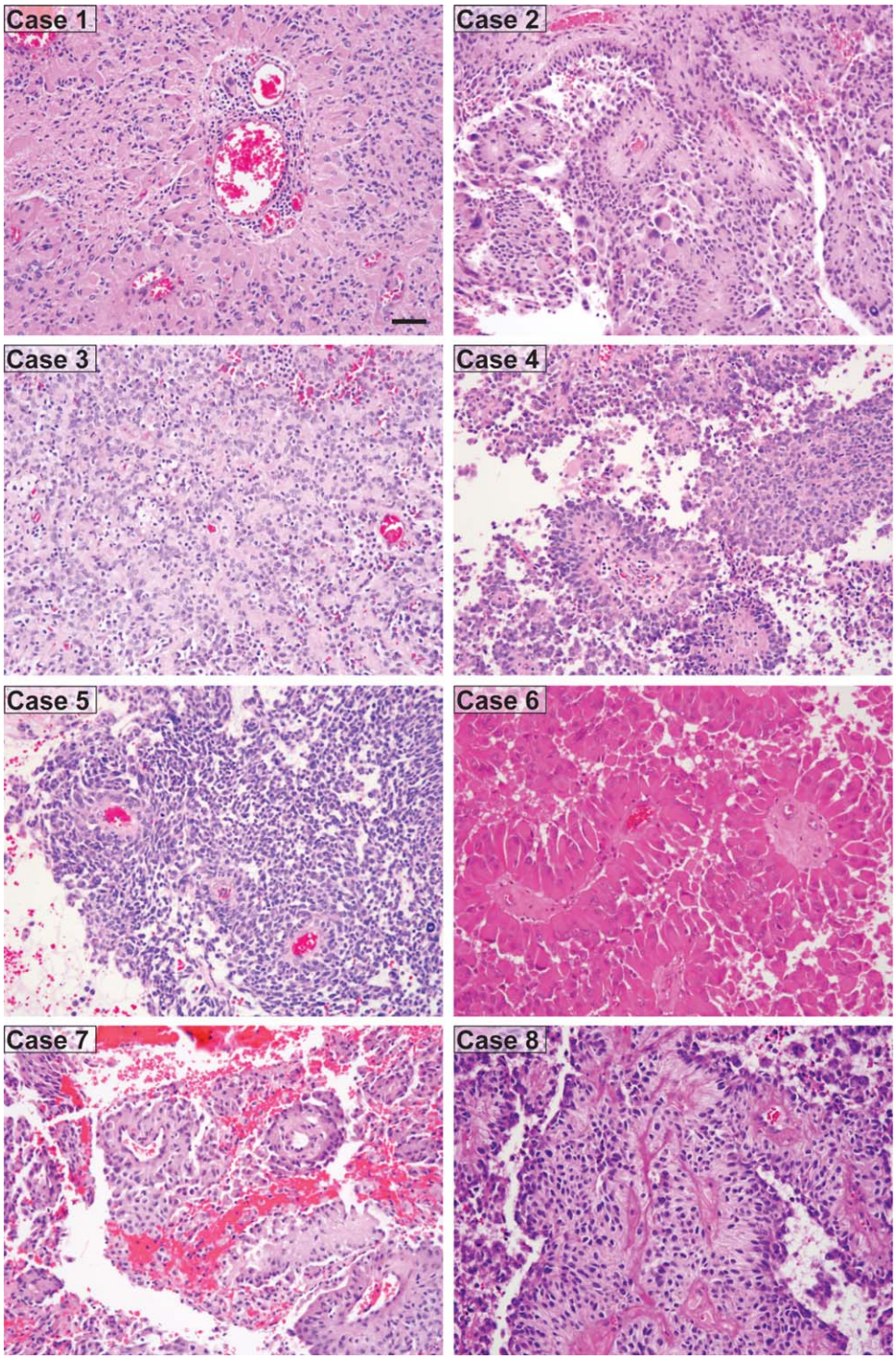

Figure 1. *Histologic features of astroblastoma cases.* Case numbers are designated in the upper left of each panel. Scale bar = 50 μm and applies to all images.

seen in Case 6). An immunohistochemical stain for L1CAM, a surrogate marker for *RELA* fusion positive cortical ependymoma, was negative in all eight cases (data not shown) (22).

Targeted next-generation sequencing results

We separated cases into three molecular/pathologic categories based on data from the UCSF 500 Cancer Panel and the FISH results (Table 3). The first category includes both of the pediatric tumors in this series (Cases 3 and 4), and two cases from adult patients (Cases 1 and 8). Tumors in this molecular category showed evidence of an *MN1* alteration by FISH and in 3 of 4 cases, the tumors grouped with CNS-HGNET-*MN1* tumors by genome-wide DNA methylation profiling (Case 1 was not classifiable by methylation profiling). Tumors in the second category (Cases 5 and 7) were clinically aggressive, showed no evidence of *MN1* alteration

© 2017 International Society of Neuropathology

Table 2. Immunohistochemical features of astroblastoma cases. See *Supporting Information* Figure S1 for representative images.

Case	GFAP	OLIG2	EMA
1	Strong, diffuse positive	Patchy positive	Focal paranuclear dot-like positive
2	Patchy positive	Positive	Patchy cytoplasmic positive
3	Scattered positive cells	Widespread positive	Widespread membranous positive
4	Strong, diffuse positive	Negative	Focal paranuclear dot-like positive
5	Rare positive cells, majority negative	Negative	Patchy membranous positive
6	Strong, diffuse positive	Negative	Admixed cytoplasmic, membranous and paranuclear dot-like positive
7	Strong, diffuse positive	Positive	Widespread cytoplasmic and membranous positive
8	Scattered positive cells	Widespread positive	Cytoplasmic and paranuclear dot-like positive

by FISH and had genetic changes that were more compatible with a diagnosis of high-grade astrocytoma, which was concordant with DNA methylation profiling in one case (the second was not classifiable by methylation profiling). The final category of tumors (Cases 2 and 6) also showed no evidence of *MN1* alteration by FISH, but unlike the second category, there were no characteristic pathogenic alterations to suggest an alternative diagnosis and tumors did not group with a known molecular entity by DNA methylation profiling. Cases 5, 6 and 8 included DNA sequencing of non-neoplastic tissue, which did not reveal any pathogenic germline mutations. The following sections describe the molecular features of the cases in each of these categories, and details of the molecular findings are provided in *Supporting Information* Table S1.

Features of category 1: Tumors with MN1 alteration

All cases in this category showed breakapart of the *MN1* locus by FISH, with a minimum of 38% of nuclei showing an abnormal FISH signal, compared to an average of 9.3% in controls (range 8% to 11%, n = 3, Figure 3A). Three of these cases grouped with CNS-HGNET-*MN1* by DNA methylation profiling, while one case could not be classified using this technique (Table 3). The immunophenotype of these tumors varied considerably from case to case, as described in Table 2 and pictured in *Supporting Information* Figure S1. The only consistent finding was that all cases showed at least focal EMA staining, albeit with a highly variable distribution and pattern (Figure 3B).

In Case 1, molecular profiling showed loss of chromosome 9, with an additional focal deep deletion on 9p21 encompassing *CDKN2A/B*, and focal losses on chromosomes 22 (Figure 3C). Case 1 also showed a guanine to alanine (G > A) transition in the *TERT* promoter at chromosome 5 position g.1,295,250 [mutant allele frequency (MAF) 28%, 664 reads]. This hotspot mutation, located 146 base pairs upstream of the *TERT* translation start site, results in re-expression of the catalytic subunit of telomerase by creating a novel consensus site for an ETS transcription factor (7, 12). Case 1 also had a subclonal variant of uncertain significance (VUS) in *NOTCH1* (p.G2262S, 27% MAF, 289 reads), classified as such because this alteration has not been reported in human cancer and occurs outside a functional domain of the protein. This case did not cluster with a specific molecular entity by methylation profiling.

In Case 8, we identified a pathogenic frameshift mutation in *ATM* (p.V1153fs) without loss of the remaining wild-type allele

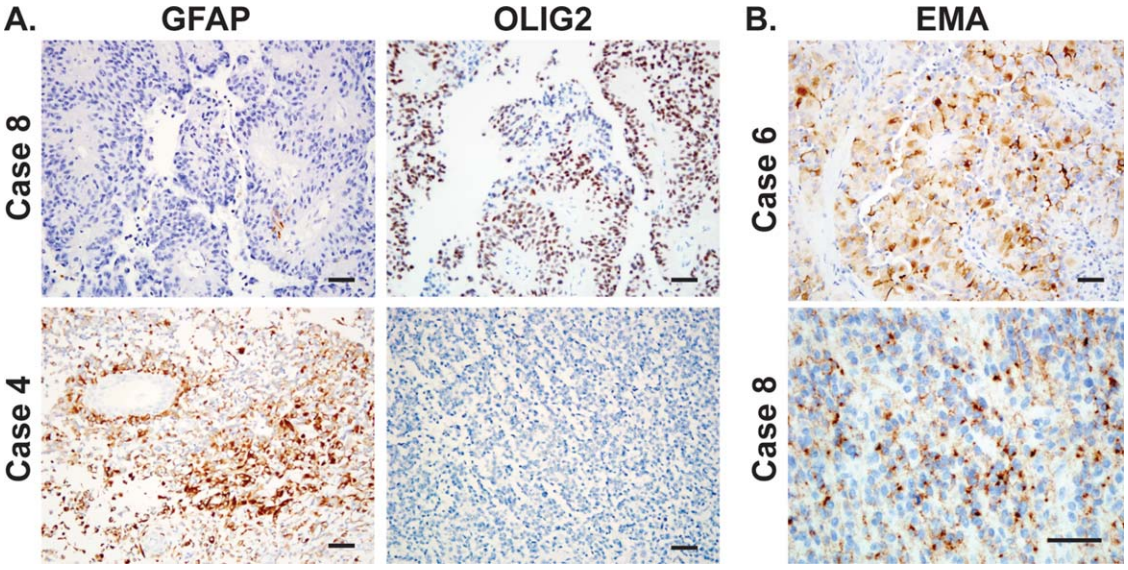

Figure 2. *Examples of immunohistochemical variability in tumors diagnosed as astroblastoma.* Scale bars = 50 μm. **A.** GFAP and OLIG2 show a reciprocal pattern of staining in some cases. **B.** The EMA pattern varies from focal paranuclear dot-like staining, to a combination of membranous, cytoplasmic and paranuclear dot-like staining.

© 2017 International Society of Neuropathology

Table 3. Molecular categories of astroblastoma cases. Abbreviations: CNS-HGNET-*MN1* = CNS high-grade neuroepithelial tumor with *MN1* alteration; FISH = fluorescence in situ hybridization; PXA = pleomorphic xanthoastrocytoma.

Case	Category	UCSF 500 pathogenic alterations	*MN1* FISH	DNA methylation profiling
1	*MN1* breakapart	*CDKN2A/B* deep deletion, *TERT* promoter mutation	Breakapart	Unclassifiable
2	Unclassifiable	*TP53*, *PTEN* mutations, numerous chromosome losses	Intact, monosomy 22q	Unclassifiable
3	*MN1* breakapart	None identified	Breakapart	CNS-HGNET-*MN1*
4	*MN1* breakapart	None identified	Breakapart	CNS-HGNET-*MN1*
5	High-grade astrocytoma	*TP53*, *NRAS*, *TERT* promoter mutations, *CDK4* amplification, chromosome 7 gain/chromosome 10 loss	Intact	Unclassifiable
6	Unclassifiable	*TP53* mutation, numerous chromosome losses	Intact, polysomy 22q	Unclassifiable
7	High-grade astrocytoma	*BRAF* p.V600E, *CDKN2A/B* deep deletion, *TERT* promoter mutation	Intact, monosomy 22q	Anaplastic PXA
8	*MN1* breakapart	*ATM* mutation, *NF2* structural rearrangement	Breakapart	CNS-HGNET-*MN1*

(43% MAF, 663 reads), as well as a complex chromosome 22 rearrangement involving the *NF2* gene and a distal portion of 22q (Figure 3D, 166 reads). Case 8 also showed a FISH pattern characterized by separation of the *MN1* centromeric (green) and telomeric (red) probes, with frequent splitting of the isolated green probe signal (Figure 3A). This case grouped with CNS-HGNET-*MN1* by methylation profiling.

In Cases 3 and 4, no pathogenic alterations were identified by sequencing. Both cases had a few nonspecific focal copy number alterations (*Supporting Information* Figure S2), and in Case 4 a subclonal VUS in *NOTCH3* was seen, which has not been reported in human cancer and occurred outside a functional domain of the protein (p.R2145L, 34% MAF, 217 reads). Interestingly, both cases showed losses on chromosome 22, and overall the only pathogenic alteration identified was by *MN1* breakapart by FISH. Both cases grouped with CNS-HGNET-*MN1* by methylation profiling.

Two cases from this category have at least 5 years of clinical follow-up. In those cases, the tumors showed a locally relapsing course despite radiation therapy: one patient is alive almost 30 years after her initial diagnosis after three repeat resections for locally recurrent tumor (Case 3), while the other died from disease 15 years after his first surgical resection, also after three local recurrences (Case 1). For two cases with limited follow-up, the patients are currently free of recurrent disease at 1 and 4 years post-resection (Cases 8 and 4, respectively), following treatment with temozolomide and radiation therapy.

Features of category 2: High-grade astrocytoma originally diagnosed as astroblastoma

Case 7 was diagnosed on a biopsy specimen from a left occipital lobe mass in a 73-year-old man. Sections showed a solid, GFAP-positive glial neoplasm with perivascular pseudorosettes, but lacking hyalinization. Genetic profiling revealed a deep deletion on chromosome 9p21 encompassing *CDKN2A/B*, along with a *TERT* promoter mutation (g.1,295,228G > A, 23% MAF, 165 reads) and *BRAF* p.V600E mutation (40% MAF, 926 reads). Variants of uncertain significance were identified in *FGFR2, FGFR4* and *NSD1* (*Supporting Information* Table S1), all at subclonal mutant allele frequency and resulting in missense mutations either of unclear clinical/biological significance (*FGFR2*) or not reported in human cancer (*FGFR4*, *NSD1*). FISH for *MN1* was intact, with 91% of tumor cells showing a single fused signal, consistent with the sequencing finding of chromosome 22 loss. Overall, the molecular findings were most compatible with anaplastic pleomorphic xanthoastrocytoma, which was confirmed by DNA methylation profile grouping which demonstrated a calibrated concordance score of 0.99 to pleomorphic xanthoastrocytoma. Analysis of a subsequent resection specimen, performed on a research basis in the context of the molecular findings, showed focal CD34 immunopositivity and pericellular reticulin deposition, consistent with this diagnosis (*Supporting Information* Figure S3). The resection specimen also showed vascular proliferation and palisading necrosis; eosinophilic granular bodies were not seen.

Case 5 occurred in a 25-year-old man with an enhancing temporal lobe mass. Sections showed a primitive-appearing neoplasm with greater than 40 mitotic figures in 10 high-power fields and an angiocentric growth pattern. No infiltrating component was seen in the adjacent uninvolved brain, and neurofilament immunohistochemistry was negative for entrapped axons within the tumor. Focal staining for MAP2 supported a glial or glioneuronal neoplasm (data not shown). Rare tumor cells stained for GFAP, but the majority of the tumor was negative for this marker. Pertinent genetic findings included trisomy of chromosome 7 and monosomy of chromosome 10, *TERT* promoter mutation (g.1,295,228G > A, 40% MAF, 138 reads), *TP53* p.F270L mutation with loss of the wild-type allele (82% MAF, 254 reads), *NRAS* p.Q61K mutation (44% MAF, 600 reads) and focal high-level amplification of *CDK4* on chromosome 12q (*Supporting Information* Figure S4). Incorporating the genetic findings with the tumor histology and immunohistochemistry, this case is most compatible with an IDH-wildtype glioblastoma with a primitive neuronal component. Such cases can show complete loss of staining for glial markers (10% of cases), are typically more circumscribed, and frequently show loss of chromosome 10 (24). While Ras-MAPK signaling pathway alterations are very common in IDH-wildtype glioblastoma, it is most typically via *NF1*

© 2017 International Society of Neuropathology

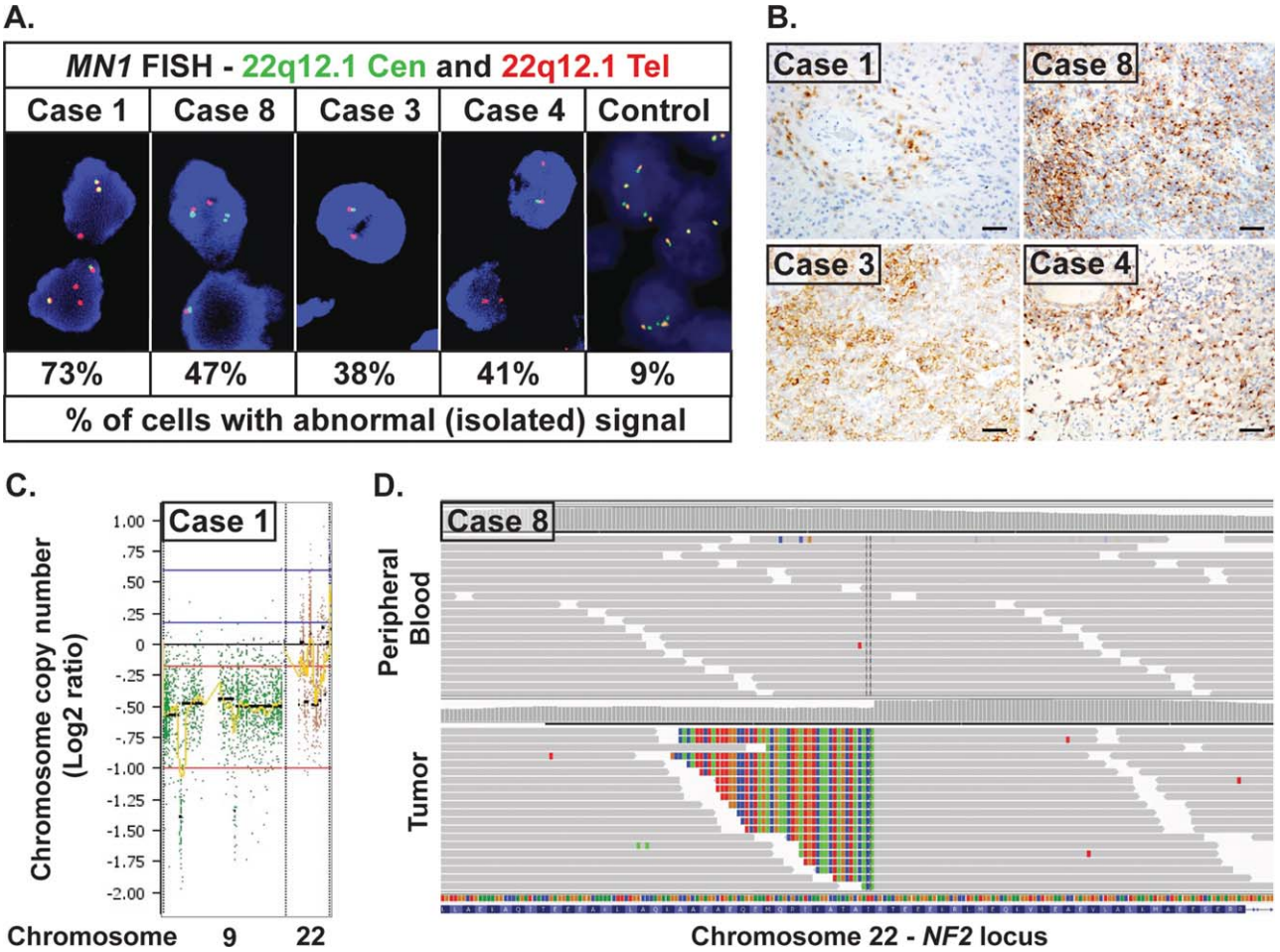

Figure 3. *Molecular features of cases classified as MN1 breakapart tumors.* **A.** Representative FISH results using an *MN1* breakapart probe, and quantitation of abnormal signal frequency in 100 examined nuclei. **B.** Variability of EMA immunohistochemical staining in this category of cases. The finding in Case 1 was isolated to a single focus in the tumor. Scale bars = 50 μm. **C.** Copy number profiling for selected chromosomes from Case 1 demonstrate homozygous deletion of *CDKN2A/B* on chromosome 9p21, and focal copy number loss on chromosome 22. **D.** Complex structural rearrangement of chromosome 22 involving the *NF2* locus in Case 8. Gray bars represent sequencing reads with homology to the displayed region, and colored bars represent transition to an area of mismatch, which corresponded to a distal region of chromosome 22q.

inactivation or growth factor receptor alterations as opposed to the *NRAS* mutation observed in this tumor. DNA methylation profiling for this case did not show grouping with a specific entity.

Both tumors in this category showed an aggressive clinical course, with rapid tumor recurrence 1–2 years after resection, despite radiation therapy.

Features of category 3: Unclassifiable cases

Two tumors, both occurring in adult patients, showed a prominent rhabdoid cell component and striking perivascular hyalinization, which was extensive in Case 6 and focal in Case 2 (Figure 4A,B). Copy number profiling showed numerous whole chromosome losses, with many shared losses occurring in both cases (Figure 4C,D). *MN1* FISH was intact in both tumors. In Case 2, FISH showed a single fused signal in most nuclei, consistent with loss of chromosome 22 (Figure 4E), and sequencing showed a *TP53* p.K132T mutation (62% MAF, 519 reads) and subclonal *PTEN* p.C136Y mutation (24% MAF, 669 reads). In Case 6, FISH showed two intact signals in most nuclei, with 25% of cells showing extra fused signals, indicative of polysomy 22 (Figure 4E) and sequencing showed a *TP53* p.G245S mutation (45% MAF, 431 reads). No pathogenic fusions, amplifications or deep deletions were seen in either case. DNA methylation profiling was unable to classify these tumors. Both patients had a good clinical outcome, with no recurrence after more than 5 years of follow-up following radiation treatment alone (Case 2) or radiation plus temozolomide (Case 6). The molecular features identified in this series and the final proposed tumor classifications are pictured in Figure 5.

DISCUSSION

In this study, we retrospectively examined the molecular underpinnings of eight tumors diagnosed histologically as astroblastoma,

© 2017 International Society of Neuropathology

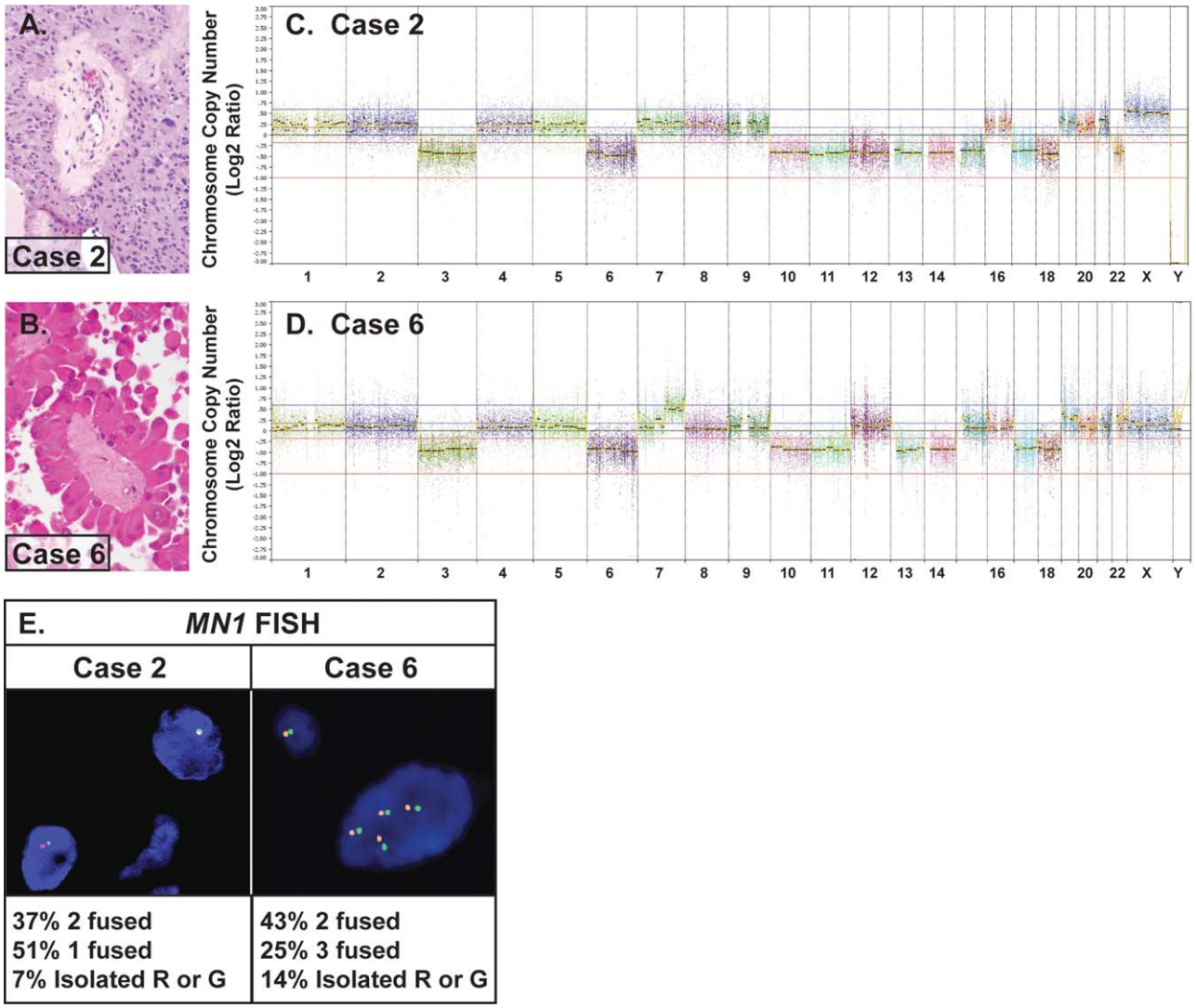

Figure 4. *Key findings in astroblastoma tumors where molecular studies are not able to definitively reclassify the tumors.* Case 2 demonstrated focal extensively hyalinized vessels (**A**) and numerous whole chromosome losses (**C**). Case 6 demonstrated extensive vascular hyalinization (**B**) and numerous whole chromosome losses (**D**). **E.** FISH studies were negative for *MN1* breakapart in both cases, but showed the indicated 22q copy number changes in a subset of cells.

and identified significant molecular heterogeneity in these cases. Our findings have important implications for predicting clinical behavior in these rare tumors. Half of the tumors in our series align with the "CNS high-grade neuroepithelial tumor with *MN1* alteration" (CNS-HGNET-*MN1*) recently defined by Sturm *et al* (25). We saw a prolonged clinical course in two of our *MN1* altered tumors, often with multiple local tumor recurrences, which is in accordance with the clinical behavior of this entity as observed in their study. Ours is the second study to suggest a prolonged overall survival in *MN1* altered neuroepithelial tumors.

Importantly, two of our *MN1* intact cases (defined by FISH) showed genetic features of high-grade astrocytoma (specifically, anaplastic pleomorphic xanthoastrocytoma and IDH-wildtype glioblastoma), and both of these tumors had an aggressive clinical course. When viewed in light of the molecular findings, we observed that both of these cases had perivascular astroblastomatous pseudorosettes, but lacked hyalinization. Faced with these histologic features, careful consideration of a high-grade astrocytoma is warranted in the differential diagnosis of astroblastoma, especially in a biopsy. Examining the genetic features of a tumor with next-generation techniques can also alert the pathologist to identify this diagnostic pitfall.

Our study widens the spectrum of genetic changes seen so far in *MN1* altered neuroepithelial tumors. Specifically, we identified a pathogenic *TERT* promoter mutation in one tumor that was confirmed by FISH to have *MN1* breakapart. Interestingly, this case was not classifiable by DNA methylation profiling, suggesting that not all *MN1*-altered neuroepithelial tumors cluster with the CNS-HGNET-*MN1* entity. Another case in our series with *MN1* breakapart by FISH that clustered with CNS-HGNET-*MN1* by methylation profiling showed a complex structural alteration involving the *NF2* gene. This is an intriguing finding because a

© 2017 International Society of Neuropathology

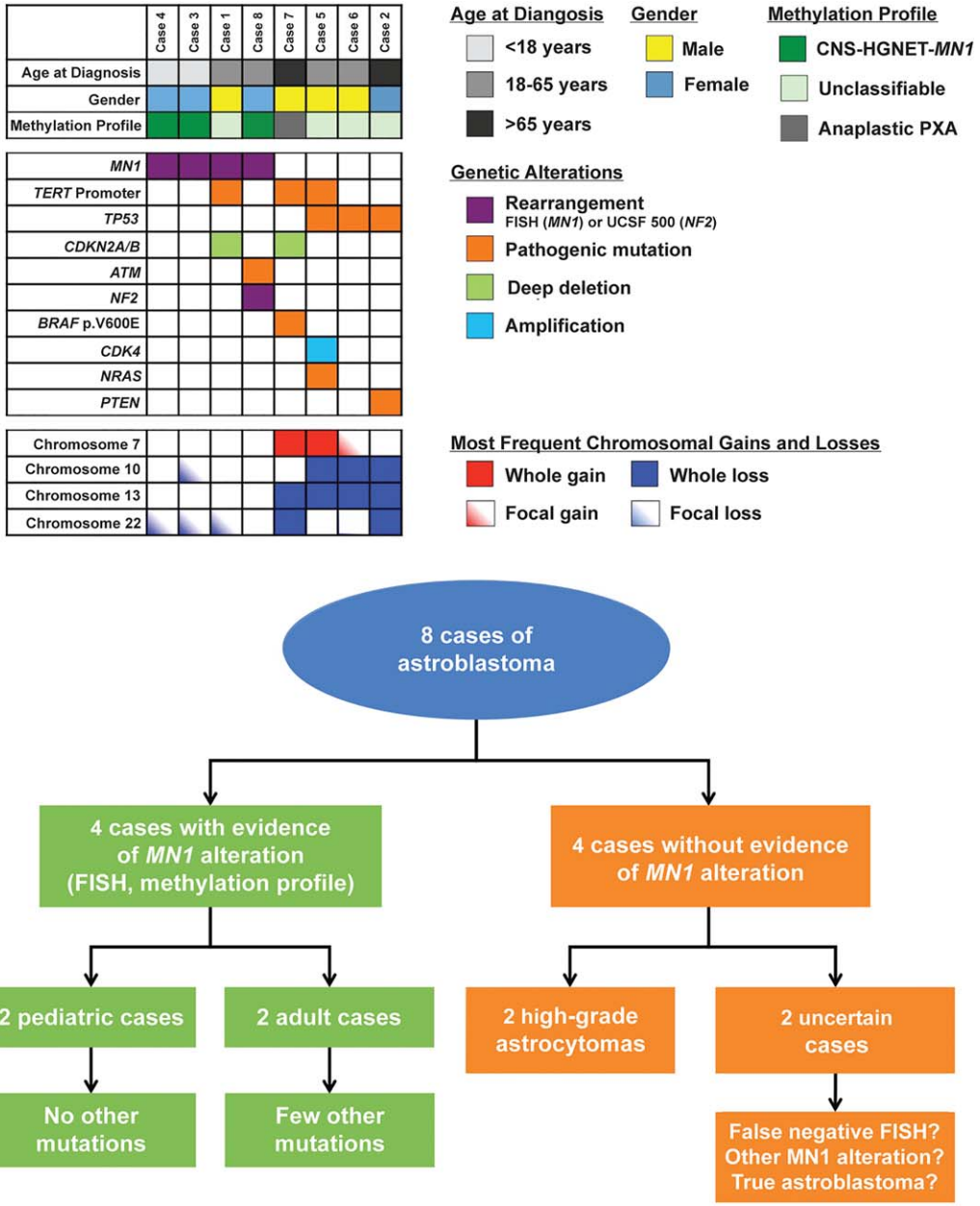

Figure 5. *Summary of molecular findings (top) and grouping of astroblastoma cases (bottom) by next-generation molecular profiling.*

relationship between astroblastoma and ependymal or tanycytic cells has been proposed based on ultrastructural and immunophenotypic studies, and *NF2* alterations are common in a subset of ependymomas arising in the spinal cord or cervicomedullary junction (16, 18, 21).

We confirmed other genetic findings that have previously been seen in CNS-HGNET-*MN1* or astroblastoma. Specifically, loss of *CDKN2A/B* occurred in one case from our series, and has been previously reported in one CNS-HGNET-*MN1* identified by DNA methylation profiling (25). We also identified a pathogenic mutation in *ATM* in one case; this feature was reported in one anaplastic astroblastoma that was analyzed by next-generation sequencing (5). Interestingly, the genetic alterations involving *CDKN2A/B, ATM, NF2* and the *TERT* promoter all occurred in tumors from adult patients. By contrast, two tumors from pediatric patients that grouped with CNS-HGNET-*MN1* by methylation profiling and had *MN1* breakapart by FISH had no other identifiable pathogenic alterations. Our findings suggest that the spectrum of genetic changes in *MN1*-altered neuroepithelial tumors could differ between pediatric and adult disease. Detailed genetic study of additional cases is required to confirm our findings.

Two cases in our series were difficult to classify, despite multiple molecular analyses. Intriguingly, these tumors share some clinical, histologic and molecular features: both tumors showed a pathogenic *TP53* mutation, numerous whole chromosome copy number alterations, occurred in adult patients and had an epithelioid/

© 2017 International Society of Neuropathology

rhabdoid morphology with some discohesive cells. This histologic pattern has been described in several astroblastoma case reports (in addition to one included in this study) and could be associated with a favorable prognosis, as we saw in our cases (6, 11, 28). Surprisingly, neither DNA methylation profiling nor FISH suggested that these two tumors have an *MN1* alteration, although we cannot exclude the possibility of an *MN1* abnormality that cannot be detected by breakapart FISH in these cases. The *PTEN* p.C136Y alteration identified in Case 2 could suggest a high-grade glioma, as this is a recurrent mutation in IDH-wildtype glioblastoma (10). However, this patient survived for over 8 years after her initial resection with no tumor recurrence after radiation therapy alone—a highly unusual clinical course for GBM—and no additional molecular or histologic features of high-grade glioma were identified.

Like any retrospective examination of a rare tumor, our study has limitations. Due to the small sample size, caution is warranted in extrapolating our findings—especially the clinical outcomes of the *MN1* altered tumors. At the time that these cases were analyzed, *MN1* was not targeted for sequencing on the NGS panel, so an exact *MN1* breakpoint or fusion partner could not be obtained. We therefore defined *MN1* alterations by breakapart FISH, but we do not have sequencing data across the *MN1* locus to confirm an abnormality and characterize the location of the breakpoint or fusion partner (attempts at RT-PCR to detect the most common *MN1-BEND2* fusion transcripts were not successful due to difficulty in obtaining high-quality mRNA from FFPE tissues). We included cases in our series that did not meet the diagnostic criteria for astroblastoma when the WHO criteria are strictly applied. Specifically, two of our cases lacked convincing hyalinization, and in these cases the diagnosis was based on astroblastomatous rosettes occurring throughout a solid glial neoplasm and excluding other diagnostic possibilities. Our molecular analysis revealed that both of these cases are actually high-grade astrocytomas that have histologic features of astroblastoma. This also occurred in one of four sequenced cases reported by Bale *et al* (5). We believe these cases have value and should be included in a retrospective molecular study because they illustrate a diagnostic pitfall that has significant clinical implications. They also demonstrate the utility of next-generation molecular studies to identify more specific tumor entities in cases with rare or ambiguous histology.

In summary, this molecular study of a series of eight previously diagnosed astroblastomas separated most cases into more specific molecularly defined entities, most frequently the recently identified CNS high-grade neuroepithelial tumor with *MN1* alteration. We identified two cases of high-grade astrocytoma with histologic features of astroblastoma in this series; such cases are important to identify due to the worse clinical outcome. Two cases in this series remain unclassifiable after detailed molecular study, including genome-wide DNA methylation profiling, a powerful technique for grouping tumors into known molecular categories. This raises the possibility that another rare and yet to be molecularly characterized astroblastoma variant exists. Taken together, our results add further evidence to support "astroblastoma" as a morphologic pattern that can be seen across a spectrum of molecularly distinct tumor entities. It remains possible that a subset of cases has a shared, distinct molecular alteration that we were not able to identify. These cases could represent a distinct diagnostic group that shows astroblastoma histologic features where the underlying genetic driver is not known, and the possibility of a common genetic underpinning for this subset of tumors warrants further study. Separation of astroblastoma into more specific molecularly defined subgroups likely explains the clinical unpredictability and difficulty in grading of these tumors.

AUTHOR CONTRIBUTIONS

MDW and DAS conceived of the study, performed the assays, and analyzed the data. MDW assembled the cases, prepared the figures, and wrote the paper. AP, GC, CT, C Pu, C Payne, AY, and SB provided specimens and clinical data. MDW, TT, AP, and DAS performed pathologic review. DAS funded the study.

CONFLICT OF INTEREST

The authors have no conflicts of interest to declare.

ACKNOWLEDGMENTS

MDW is supported by an NIH T32 grant (CA151022). DAS is supported by an NIH Director's Early Independence Award (DP5 OD021403) and the UCSF Physician-Scientist Scholar Program. The authors thank Dr. Andrey Korshunov for assistance with the DNA methylation array data interpretation, Jie Hou for assistance in performing and interpreting the FISH studies, Dr. Joanna Phillips and Dr. Joydeep Mukherjee for their comments and discussions, and the UCSF Clinical Cancer Genomics Laboratory for performing the NGS. This work was presented in part at the 93rd Annual Meeting of the American Association of Neuropathologists in Garden Grove, CA, in June 2017.

REFERENCES

1. Ahmed KA, Allen PK, Mahajan A, Brown PD, Ghia AJ (2014) Astroblastomas: a surveillance, epidemiology, and end results (SEER)-based patterns of care analysis. *World Neurosurg* **82**:e291–e297.
2. Asha U, Mahadevan A, Sathiyabama D, Ravindra T, Sagar BKC, Bhat DI *et al* (2015) Lack of IDH1 mutation in astroblastomas suggests putative origin from ependymoglial cells?. *Neuropathology* **35**: 303–311.
3. Bailey PS, Bucy PC (1930) Astroblastomas of the brain. *Acta Psychiat Scand* **5**:439–461.
4. Bailey PS, Cushing H (1930) *A Classification of Tumors of the Glioma Group on a Histogenetic Basis with a Correlation Study of Prognosis*. Lippincott: Philadelphia.
5. Bale TA, Abedalthagafi M, Bi WL, Kang YJ, Merrill P, Dunn IF *et al* (2016) Genomic characterization of recurrent high-grade astroblastoma. *Cancer Genet* **209**:321–330.
6. Bannykh SI, Fan X, Black KL (2007) Malignant astroblastoma with rhabdoid morphology. *J Neurooncol* **83**:277–278.
7. Bell RJA, Rube HT, Kreig A, Mancini A, Fouse SD, Nagarajan RP *et al* (2015) Cancer. The transcription factor GABP selectively binds and activates the mutant TERT promoter in cancer. *Science* **348**: 1036–1039.
8. Bonnin JM, Rubinstein LJ (1989) Astroblastomas: a pathological study of 23 tumors, with a postoperative follow-up in 13 patients. *Neurosurgery* **25**:6–13.
9. Brat DJ, Hirose Y, Cohen KJ, Feuerstein BG, Burger PC (2000) Astroblastoma: clinicopathologic features and chromosomal

© 2017 International Society of Neuropathology

abnormalities defined by comparative genomic hybridization. *Brain Pathol* **10**:342–352.
10. Brennan CW, Verhaak R, McKenna A, Campos B (2013) The somatic genomic landscape of glioblastoma. *Cell* **155**:462–477.
11. Fathi A-R, Novoa E, El-Koussy M, Kappeler A, Mariani L, Vajtai I (2008) Astroblastoma with rhabdoid features and favorable long-term outcome: report of a case with a 12-year follow-up. *Pathol Res Pract* **204**:345–351.
12. Huang FW, Hodis E, Xu MJ, Kryukov GV, Chin L, Garraway LA (2013) Highly recurrent TERT promoter mutations in human melanoma. *Science* **339**:957–959.
13. Janz C, Buhl R (2014) Astroblastoma: report of two cases with unexpected clinical behavior and review of the literature. *Clin Neurol Neurosurg* **125**:114–124.
14. Kline CN, Joseph NM, Grenert JP, van Ziffle J, Talevich E, Onodera C *et al* (2017) Targeted next-generation sequencing of pediatric neuro-oncology patients improves diagnosis, identifies pathogenic germline mutations, and directs targeted therapy. *Neuro-oncology* **19**:699–709.
15. Korshunov A, Ryzhova M, Hovestadt V, Bender S, Sturm D, Capper D *et al* (2015) Integrated analysis of pediatric glioblastoma reveals a subset of biologically favorable tumors with associated molecular prognostic markers. *Acta Neuropathol* **129**:669–678.
16. Kubota T, Sato K, Arishima H, Takeuchi H, Kitai R, Nakagawa T (2006) Astroblastoma: immunohistochemical and ultrastructural study of distinctive epithelial and probable tanycytic differentiation. *Neuropathology* **26**:72–81.
17. Lau PPL, Thomas TMM, Lui PCW, Khin AT (2006) "Low-grade" astroblastoma with rapid recurrence: a case report. *Pathology* **38**: 78–80.
18. Lehman NL (2008) Central nervous system tumors with ependymal features: a broadened spectrum of primarily ependymal differentiation?. *J Neuropathol Exp Neurol* **67**:177–188.
19. Lehman NL, Hattab EM, Mobley BC, Usubalieva A, Schniederjan MJ, McLendon RE *et al* (2017) Morphological and molecular features of astroblastoma, including BRAFV600E mutations, suggest an ontological relationship to other cortical-based gliomas of children and young adults. *Neuro-oncology* **19**:31–42.
20. Louis DN, Ohgaki H, Wiestler OD, Cavanee WK, eds (2016) *World Health Organization Classification of Tumors of the Central Nervous System*, revised 4th edn. International Agency for Research on Cancer: Lyon, France.
21. Pajtler KW, Witt H, Sill M, Jones DTW, Hovestadt V, Kratochwil F *et al* (2015) Molecular classification of ependymal tumors across all CNS compartments, histopathological grades, and age groups. *Cancer Cell* **27**:728–743.
22. Parker M, Mohankumar KM, Punchihewa C, Weinlich R, Dalton JD, Li Y *et al* (2014) C11orf95-RELA fusions drive oncogenic NF-κB signalling in ependymoma. *Nature* **506**:451–455.
23. Payne C, Batouli A, Stabingas K, Alcindor D, Abdel Aziz K, Pu C *et al* (2017) A pediatric tumor found frequently in the adult population: a case of anaplastic astroblastoma in an elderly patient and review of the literature. *Case Rep Neurol Med* **2017**:1607915.
24. Perry A, Miller CR, Gujrati M, Scheithauer BW, Zambrano SC, Jost SC *et al* (2009) Malignant gliomas with primitive neuroectodermal tumor-like components: a clinicopathologic and genetic study of 53 cases. *Brain Pathol* **19**:81–90.
25. Sturm D, Orr BA, Toprak UH, Hovestadt V, Jones DTW, Capper D *et al* (2016) New brain tumor entities emerge from molecular classification of CNS-PNETs. *Cell* **164**: 1060–1072.
26. Talevich E, Shain AH, Botton T, Bastian BC (2016) CNVkit: genome-wide copy number detection and visualization from targeted DNA sequencing. *PLoS Comput Biol* **12**:e1004873.
27. Thiessen B, Finlay J, Kulkarni R, Rosenblum MK (1998) Astroblastoma: does histology predict biologic behavior?. *J Neurooncol* **40**:59–65.
28. Yuzawa S, Nishihara H, Tanino M, Kimura T, Moriya J, Kamoshima Y *et al* (2016) A case of cerebral astroblastoma with rhabdoid features: a cytological, histological, and immunohistochemical study. *Brain Tumor Pathol* **33**:63–70.

SUPPORTING INFORMATION

Additional supporting information may be found in the online version of this article at the publisher's web-site:

Figure S1. Immunohistochemical features seen across 8 cases of astroblastoma. Scale bars = 50 μm.

Figure S2. Genome-wide copy number profiles of cases 3 and 4, both pediatric tumors with *MN1* breakapart by FISH and grouping with CNS-HGNET-*MN1* by DNA methylation profiling. Material from Case 3 was a recurrent tumor, post radiation treatment.

Figure S3. Immunohistochemical and molecular features in a case that grouped as anaplastic pleomorphic xanthoastrocytoma by DNA methylation profiling, and showed an intact *MN1* locus by FISH. (A) Histologic findings on a subsequent resections specimen show focal CD34 positivity in cells with ramified processes, and focal pericellular reticulin deposition. (B) Genome-wide copy number profiling revealed deletion of *CDKN2A/B* and loss of chromosome 22. (C) *MN1* FISH demonstrates an intact signal in the vast majority of tumors cells, with most tumor cells show only one fused signal, consistent with loss of chromosome 22 seen on the next-generation sequencing copy number profile.

Figure S4. Molecular features in a case that showed genetic features of IDH-wildtype glioblastoma. (A). Genome-wide copy number profile showing key findings of trisomy of chromosome 7, monosomy of chromosome 10, and *CDK4* amplification. (B). *MN1* FISH shows an intact (ie, fused) signal in 90% of cells.

Table S1. Summary of NGS findings. MAF = Mutant allele frequency, N/A = Not applicable, VUS = Variant of uncertain significance.

© 2017 International Society of Neuropathology